A Simple Stochastic Model for Generating Broken Cloud Optical Depth and Cloud-Top Height Fields

SERGEI M. PRIGARIN

Novosibirsk State University, and Institute of Computational Mathematics and Mathematical Geophysics, Russian Academy of Sciences (Siberian Branch), Novosibirsk, Russia

ALEXANDER MARSHAK

NASA Goddard Space Flight Center, Climate and Radiation Branch, Greenbelt, Maryland

(Manuscript received 4 December 2007, in final form 19 May 2008)

ABSTRACT

A simple and fast algorithm for generating two correlated stochastic two-dimensional (2D) cloud fields is described. The algorithm is illustrated with two broken cumulus cloud fields: cloud optical depth and cloud-top height retrieved from the Moderate Resolution Imaging Spectroradiometer (MODIS). Only two 2D fields are required as an input. The algorithm output is statistical realizations of these two fields with approximately the same correlation and joint distribution functions as the original ones. The major assumption of the algorithm is statistical isotropy of the fields. In contrast to fractals and the Fourier filtering methods frequently used for stochastic cloud modeling, the proposed method is based on spectral models of homogeneous random fields. To retain the same probability density function as the (first) original field, the method of inverse distribution function is used. When the spatial distribution of the first field has been generated, a realization of the correlated second field is simulated using a conditional distribution matrix. This paper serves as a theoretical justification of the publicly available software "Simulation of a two-component cloud field," which has been recently released. Although 2D rather than full 3D, the stochastic realizations of two correlated cloud fields that mimic statistics of given fields have proven to be very useful to study 3D radiative transfer features of broken cumulus clouds for a better understanding of shortwave radiation and the interpretation of remote sensing retrievals.

1. Introduction

To better understand and predict shortwave radiation in realistic cloudy atmospheres, we need to specify the 3D distribution of cloud liquid water. Also, statistical cloud retrievals that include 3D radiative transfer need to be trained on a large number of 3D cloud fields (Evans et al. 2008). Realistic cloud fields and spatial distributions of cloud liquid water can be obtained from either dynamical or stochastic cloud models. Based on cloud dynamics, physical (or dynamical) cloud models such as a large-eddy simulation (LES) or a cloud-resolving model (e.g., Ackerman et al. 1995) are physically consistent but require specification of a lot of atmospheric parameters and often are computationally expensive. On the other hand, stochastic cloud models based on aircraft, satellite, or ground measurements of cloud structure are computationally inexpensive and can output a much larger range of scales than dynamical models. Stochastic cloud models are mostly 2D because currently there are no techniques to measure a full 3D cloud structure. (To get a 3D stochastic model, one can assume the same statistics for both horizontal directions; see Evans and Wiscombe 2004; Hogan and Kew 2005.)

Over the last two decades, many different cloud stochastic models have been developed. We break them into two classes. The first class of cloud models uses only a few parameters to simulate the main aspects of the realistic cloud fields like the mean, standard deviation, and correlation (often assumed to be a power law). These models are very simple and are generally used to test hypotheses and better understand cloud–radiation interaction; they include the fractionally integrated cascade model (Schertzer and Lovejoy 1987), the bounded cascades (Cahalan 1994; Marshak et al. 1994), the fractional Brownian motion (Voss 1985), the Fourier filtering of Gaussian noise (Barker and Davies

―――――――

Corresponding author address: Alexander Marshak, NASA GSFC, Code 613.2, Greenbelt, MD 20771.
E-mail: alexander.marshak@nasa.gov

1992; Evans 1993; Várnai 2000), and the Poisson distribution of cloud elements (Zuev and Titov 1995), to name a few. These models generally produce an unbroken (overcast) 2D x–y field of cloud optical depth or cloud liquid water path. To obtain the desired cloud fraction, a simple threshold can be used (e.g., Barker and Davies 1992; Marshak et al. 1998).

The second class of cloud stochastic models provides a statistical reconstruction of an observed field and generates the detailed cloud structure. They are also called statistical cloud generators (Venema et al. 2006a; Schmidt et al. 2007). These cloud models are usually 3D rather than 2D. For cumulus clouds, Evans and Wiscombe (2004) used time–height radar data to generate 2D realizations of cloud liquid water that are then generalized to 3D fields assuming statistical homogeneity and horizontal isotropy. For stratocumulus clouds, Di Giuseppe and Tompkins (2003) generated 3D cloud liquid water fields by combining stochastic horizontal models based on a power spectrum and Fourier filtering (at each height) with realistic vertical profiles of total water and temperature. From radar time–height series, using a Fourier transform technique, Hogan and Kew (2005) generated realistic 3D cirrus clouds with a fallstreak structure vertically changing the slope of the power spectrum. Venema et al. (2006a,b) generated a surrogate cloud field with a liquid water distribution and spatial correlation (through a power spectrum) statistically similar to the observed one. Venema et al. (2006b) also compared radiative properties of LES clouds with their surrogate fields and Venema et al. (2006a) provided an excellent review of different cloud generators. Finally, we mention the Scheirer and Schmidt (2005) generator, which reproduces cloud fields of liquid water and effective radius using aircraft data. Schmidt et al. (2007) used cloud fields simulated by the last three generators as input to a 3D radiative transfer model to compare its output with the radiative flux measurements.

The current paper describes a simple stochastic model that belongs to the second class of cloud stochastic models. For given 2D fields of cloud optical depth and cloud-top height, the model generates realizations of these two fields with the same covariance of the cloud mask and the joint distribution as the original fields. In contrast to Evans and Wiscombe (2004), it does not generate 3D cloud liquid water fields but rather provides the x–y fields of cloud optical and geometrical thicknesses (assuming a constant cloud base). To simulate the required autocorrelation function, it uses spectral models of homogeneous random fields (Prigarin 1995, 2001) rather than commonly used Fourier filtering (e.g., Evans 1993; Di Giuseppe and Tomp-

kins 2003; Evans and Wiscombe 2004; Hogan and Kew 2005; Venema et al. 2006b). Another distinguishable feature of this paper is that it provides a theoretical background for the publicly available software that has been recently developed and released by the authors.

The plan of the paper is as follows: The next section briefly discusses two stochastic models of broken cloudiness that are based on a truncated Gaussian homogeneous field. The (auto)correlation function of a 2D field defines its structure. Section 3 describes how to generate a quasi-Gaussian field with a given correlation function that is retrieved from the covariance of the indicator function of the original field. Section 4 then explains how to modify the field to reproduce the observed distribution. In section 5 we generate the second field using the joint distribution of the given fields of cloud optical depth and cloud-top height. Section 6 illustrates the theory with Moderate Resolution Imaging Spectroradiometer (MODIS) data; section 7 summarizes the main steps of the proposed algorithm and discusses its applications. Section 8 gives a brief summary of the results. At the end, appendix A demonstrates the relations between the covariance functions of a Gaussian random filed and its indicators, and appendix B illustrates spectral models of Gaussian isotropic homogeneous random fields on the x–y plane.

2. Quasi-Gaussian model of broken cloudiness

Let us assume that our cloud field has a constant cloud base at height H_0 and a variable cloud top described by

$$w(x, y) = H_0 + \max\{a[v(x, y) - d], 0\} \quad \text{for} \quad -\infty < d < \infty.$$

(1a)

Here, $v(x, y)$ is a homogeneous Gaussian field with zero mean, unit variance, and a correlation function $K(x, y)$ [with $K(0, 0) = 1$]. The point (x, y, z) belongs to a cloud if $H_0 \leq z \leq w(x, y)$. A value $w(x, y) = H_0$ simply means that there is a cloud gap in the horizontal point (x, y). The cloud-top field w has two parameters: a and d. Parameter $a > 0$ stretches the cloud-top field vertically and parameter d defines the truncation level (cf. Marshak et al. 1998).

Simultaneously with Eq. (1a), we consider another model (Kargin and Prigarin 1988) of cloud top:

$$w(x, y) = H_0 + \max\{a[|v(x, y)| - d], 0\} \quad \text{for} \quad 0 \leq d < \infty.$$

(1b)

We will call Eqs. (1a) and (1b) models A and B, respectively. Figure 1 illustrates the difference between the two models. We can see that for model A, a positive
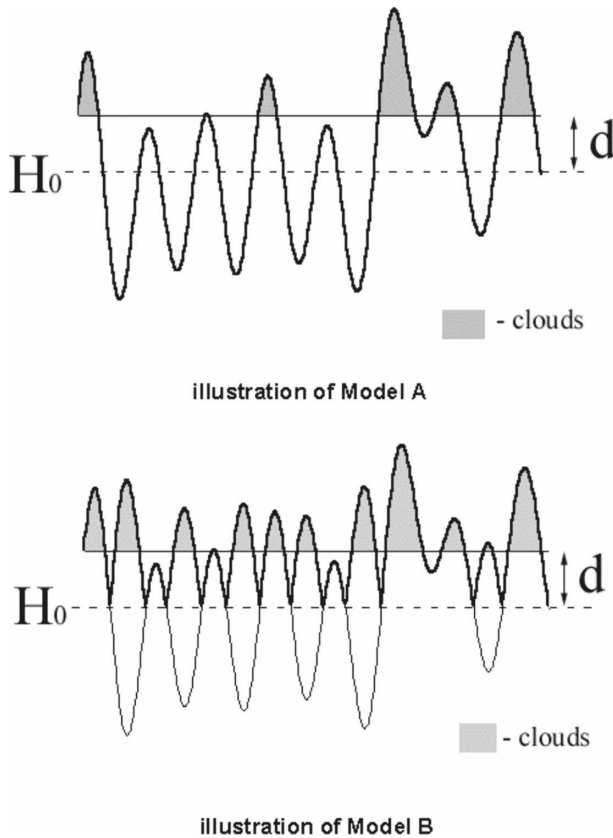
FIG. 1. A schematic illustration of models A and B; H_0 is a constant cloud base and d is a cutting threshold level.

d corresponds to a broken cloud field while a negative d corresponds rather to a more "overcast" cloud with a few gaps. Based on Fig. 1, one can say that model B better represents the cellular structure of stratocumulus whereas model A is for more broken cumulus clouds.

It can be shown that cloud fraction A_c has a different value for both models, namely:

$$A_c = P[v(x, y) > d] = 1 - \Phi(d), \quad \text{over} \quad -\infty < d < \infty,$$
$$(2a)$$

for model A and

$$A_c = P[v(x, y) > d] = 2[1 - \Phi(d)], \quad \text{over} \quad 0 \leq d < \infty,$$
$$(2b)$$

for model B, where

$$\Phi(d) = \frac{1}{\sqrt{2\pi}} \int_{-\infty}^{d} \exp\left(-\frac{x^2}{2}\right) dx$$

is the standard normal cumulative distribution function, which ranges between 0 and 0.5 for negative d and between 0.5 to 1 for positive d.
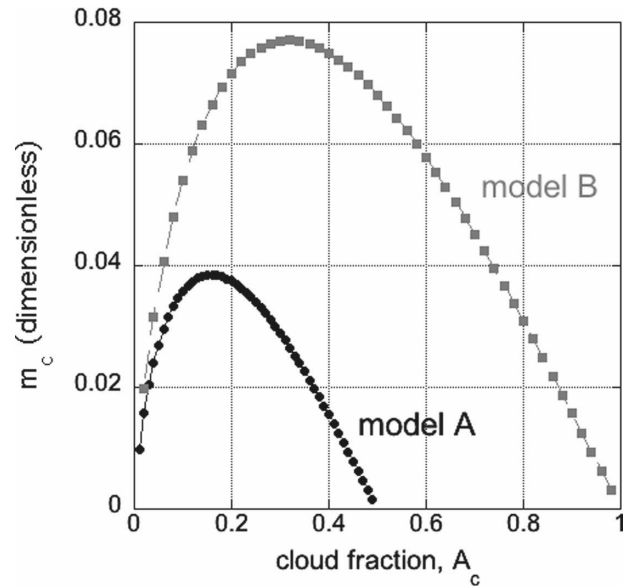

FIG. 2. Number of clouds per unit area m_c ($k = 1$), as a function of cloud fraction A_c for models A and B.

For both models, we can determine the average number of clouds m_c per unit area as a limit of the number of clouds in a convex domain of area S divided by S when S tends to infinity. Note that m_c is dimensionless. Obviously m_c will depend on d and the autocorrelation function K. For isotropic fields, one obtains [e.g., Sveshnikov 1968, Eq. (45.51), p. 441]

$$m_c = i \frac{d}{\sqrt{(2\pi)^3}} k \exp\left(-\frac{d^2}{2}\right) \quad \text{for} \quad d > 0, \quad (3)$$

where $i = 1$ for model A and $i = 2$ for model B. Here, $k > 0$ is the second derivative of $-K(x, y)$ with respect to x or y taken at $x = y = 0$ (with a negative sign). Note that for isotropic fields, the derivatives are equal [see Eq. (5) below].

Figure 2 shows the dependence of m_c on cloud fraction A_c for both models and isotropic fields. We see that the number of clouds first increases with cloud fraction and then decreases. This is because the cloud fraction A_c itself monotonically decreases with the truncation level d whereas the number of clouds m_c first increases with d and then decreases (see Fig. 1). Note that for model A, the number of clouds m_c for $A_c > 0.5$ ($d < 0$) is not defined. The generalization of Eq. (3) to anisotropic fields is straightforward (Prigarin and Marshak 2005).

To summarize, both cloud models A and B are uniquely determined by parameters a and d and a correlation function K. To simulate a cloud field with a given cloud fraction A_c, we first solve Eq. (2) for the
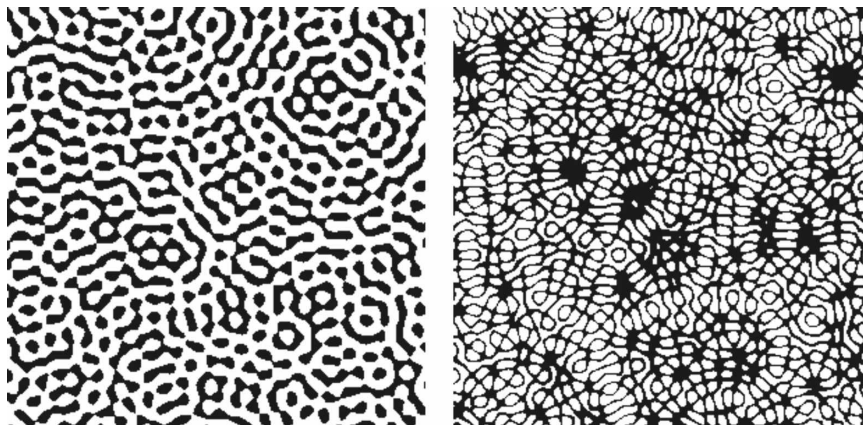
FIG. 3. Configuration of cloud fields (300 km × 300 km) for models (left) A and (right) B on the basis of a Gaussian random field with a correlation function J_0 for the same cloud fraction $A_c = 0.58$ ($\rho = 0.5$; $d = -0.20$ for model A and 0.55 for model B). To simulate a Gaussian random field, a spectral model from Prigarin (2001, section 1.1.4) was used; see also appendix B.

truncation level d. Then it is necessary to generate the correlation function $K(x, y)$ based on some additional information about correlation in a real cloud field. Parameter a is determined from a simple one-point statistic describing the cloud-top height field. The most difficult part of such an approach is the choice (or generation) of the correlation function K; it will be discussed in the next section.

Finally, we emphasize that the cloud-top height field $w(x, y)$ is simulated in two steps: (i) simulation of the Gaussian field $v(x, y)$ with mean zero and correlation function $K(x, y)$ and (ii) calculation of $w(x, y)$ with parameters a and d using (1a) or (1b). The problem of numerical simulation of Gaussian random fields has been well studied [e.g., chapters 1, 2, and 4 in Ogorodnikov and Prigarin (1996), as well as Prigarin (2001) and references therein] and will not be discussed here. Appendix B illustrates the approximation of a Gaussian homogeneous random field used in the numerical examples in section 6.

3. Correlation function

The correlation function defines the geometrical structure of a cloud field, including the size and distribution of individual clouds and the space between them. Perhaps the simplest and/or the most deterministic isotropic cloud field used in the first stochastic models can be defined by a Bessel function of the first kind, J_0 (see Gikhman and Skorokhod 1977, p. 87). In this case, the correlation function is

$$K(x, y) = J_0(\rho\sqrt{x^2 + y^2}), \qquad (4)$$

where parameter ρ is responsible for cloud sizes (the larger the value of ρ, the smaller an average cloud is). It is easy to see that

$$k = -\left.\frac{\partial^2 K(x, y)}{\partial x^2}\right|_{x=y=0} = -\left.\frac{\partial^2 K(x, y)}{\partial y^2}\right|_{x=y=0} = \frac{\rho^2}{2}. \qquad (5)$$

Thus, to define ρ, one uses Eq. (3), which relates the average number of clouds per unit area m_c and the second derivative k. Because ρ is fixed, the use of the correlation function (4) is very limited and the cloud fields based on it are unrealistic (see Fig. 3 as an example).

To generalize (4), Prigarin et al. (1998) used the radial spectral density of a Gaussian field $z(\rho)$ and a representation of the normalized correlation function as an integral over all cloud sizes ρ of a product between $z(\rho)$ and J_0:

$$K(x, y) = \int_0^\infty J_0(\rho\sqrt{x^2 + y^2})z(\rho)\, d\rho. \qquad (6)$$

Here, $z(\rho) \geq 0$ and $\int_0^\infty z(\rho)d\rho = 1$. Varying $z(\rho)$, in general, one can get any correlation function of a random isotropic field on the plane.

Below we briefly describe a general procedure for generating the correlation function $K(x, y)$ based on observations (leaving the details for appendix A). As an illustration, in section 6 we apply our algorithm to a broken cloud scene retrieved from MODIS.

Let $I(x, y)$ be an indicator function (a binary cloud mask) that takes value 1 if there is a cloud above point (x, y) and 0 otherwise. Based on observations, we can

estimate the mathematical expectation of I, which is a cloud fraction A_c:

$$A_c = E[I(x, y)] \tag{7}$$

and its covariance function,

$$K_I(x, y) = E[I(x, y)I(0, 0)]. \tag{8}$$

It is known (Ogorodnikov and Prigarin 1996, p. 65) that the covariance function $K_I(x, y)$ of the indicator field $I(x, y)$ and the correlation function $K(x, y)$ of a Gaussian field $v(x, y)$ are nontrivially related. This relationship allows us to retrieve the correlation function $K(x, y)$ from the measured covariance function $K_I(x, y)$. The main steps of the retrieval are described in appendix A. Note that the truncation level d is uniquely defined from Eqs. (2) and (7).

4. Geometrical thickness with a given density

Equations (1a) and (1b) alone do not allow us to control the distribution of cloud geometrical thickness $w(x, y) - H_0$. Determined by Eqs. (1a) and (1b), this distribution is a scaled-up ($a > 1$) or -down ($a < 1$) truncated (by a parameter d) Gaussian distribution; its density is defined by

$$f_a(h) = \frac{1}{aC} \varphi\left(\frac{h}{a} + d\right) \quad \text{for} \quad h > 0 \quad \text{and}$$
$$C = \int_d^\infty \varphi(x) \, dx, \tag{9}$$

where $\varphi(x) = 1/2\pi \exp(-x^2/2)$ is a standard Gaussian density. However, the observed distribution of cloud thickness does not necessarily satisfy Eq. (9). In general, one has to modify Eqs. (1a) and (1b) to reproduce the observed distribution. We describe below a modification of a Gaussian model that allows reproduction of any given distribution. This modification is based on the method of inverse distribution function widely used in statistical modeling (e.g., Ogorodnikov and Prigarin 1996, 65–71).

Let $g(h)$ ($h > 0$) be a density of the observed distribution of cloud thickness. We denote its distribution function by

$$G(h) = \int_0^h g(x) \, dx, \quad \text{for} \quad h > 0. \tag{10}$$

It is easy to see that if

$$F(h) = \int_0^h f_1(x) \, dx, \quad \text{for} \quad h > 0, \tag{11}$$

is the distribution function [with density $f_1(h)$ defined in Eq. (9) where $a = 1$] and x_i is a random variable dis-

tributed with the density f_1, then $G^{-1}F(x_i)$ will have a density of the observed distribution of cloud geometrical thickness. Indeed, there is a general statement (e.g., Gentle 2003, p. 42): if F is a distribution function of a random variable x_i then $F(x_i)$ is uniformly distributed on the interval (0, 1). Therefore, the random variable $G^{-1}F(x_i)$ has the probability density g. Note that a method of inverse distribution function similar to the above has been also used by Evans and Wiscombe (2004) to generate lookup tables for cloud liquid water content and droplet effective radius [see their Eq. (A.3)].

This leads us to the following modification of Eqs. (1a) and (1b):

$$w(x, y) = H_0 + G^{-1}F\{\max[v(x, y) - d, 0]\}, \quad \text{where}$$
$$-\infty < d < \infty \tag{12a}$$

for model A, and

$$w(x, y) = H_0 + G^{-1}F\{\max[|v(x, y)| - d, 0]\}, \quad \text{where}$$
$$0 \le d < \infty. \tag{12b}$$

for model B.

In contrast to (1a) and (1b), distributions of cloud thickness $w(x, y) - H_0$ defined by either (12a) or (12b) match the observed probability distribution $G(h)$. In addition, we recall that $v(x, y)$ is a homogeneous Gaussian field with zero mean and unit variance; its correlation function $K(x, y)$ is retrieved from the covariance function $K_I(x, y)$ of the observed cloud mask field $I(x, y)$. For both models, parameter d is uniquely determined from the average value of $I(x, y)$, that is, cloud fraction A_c [see (7)].

5. Joint distribution of optical and geometrical thicknesses

We assume here that we have two random variables: cloud optical depth $\tau(x, y)$ and cloud geometrical thickness $h(x, y)$. Then a pair (τ, h) will be a two-dimensional variable and $P(\tau_1 < \tau < \tau_2, h_1 < h < h_2)$ will be the probability that the values of τ and h fall in the intervals (τ_1, τ_2) and (h_1, h_2), respectively.

Practically (see next section), when two matrixes τ and h are given from observations, we first subdivide all their values into M and N bins, respectively. Then we calculate a conditional distribution matrix:

$$\mathbf{P}(m, n) = P(\tau \text{ is in } m\text{'s bin, provided } h \text{ is in } n\text{'s bin}),$$
$$m = 1, \dots, M, n = 1, \dots, N. \tag{13}$$

Now, if we assume that we have a realization of one variable, say h, then by using the conditional distribution matrix $\mathbf{P}$ we can simulate a distribution of a second variable, τ. This is a straightforward procedure similar to a simulation of random number with a given distri-
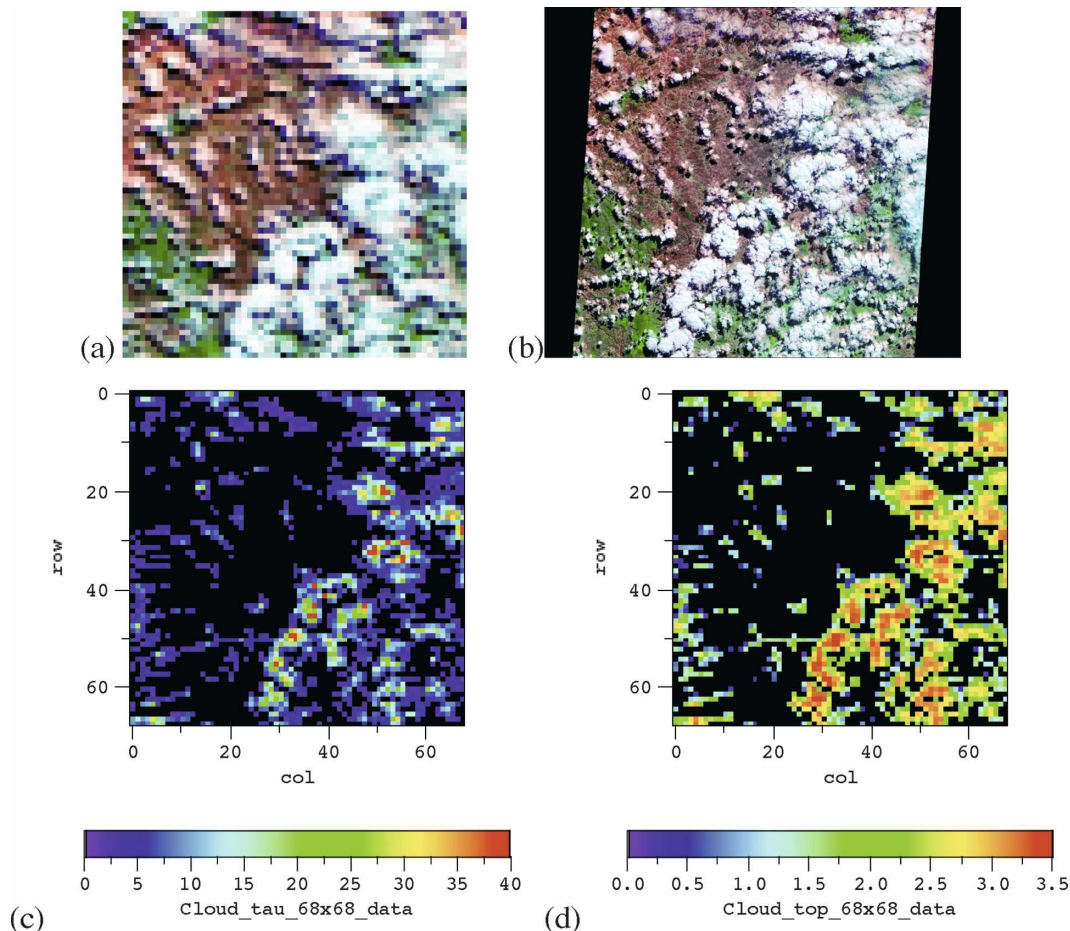
FIG. 4. A 68 km × 68 km region in Brazil centered at 17°S and 42°W collected on 9 Aug 2001 at 1015 LT. The solar zenith angle $\theta_0 = 41°$; the solar azimuth angle $\varphi_0 = 23°$ (from the top). (a) MODIS true color RGB (red–green–blue) 1-km resolution; (b) ASTER RGB 15-m resolution; (c) retrieved cloud optical thickness; (d) retrieved cloud-top height (in km).

bution. As a result for each point (x, y) we will get both $\tau(x, y)$ and $h(x, y)$ preserving conditional distribution (13) as well as the distribution of the random vector $[h(x, y), \tau(x, y)]$. The order of simulation (first τ and then h or first h and then τ) is irrelevant for the reproduction of the joint distribution of the components of this two-dimensional vector.

Note that realizations of the second component generated using a conditional distribution matrix (13) are usually more stochastic (or noisy) than the given one. This is especially well pronounced if the original field has a strong spatial heterogeneity (e.g., the highest values are localized in several neighboring pixels). In a simulated field, these high values are not necessarily well localized and sometimes can be distributed through the whole scene, making it much noisier. This problem has been discussed in more detail in Prigarin and Marshak (2008).

6. Illustration with MODIS data

To illustrate the above theory with observations, we have selected a 1-km spatial resolution MODIS 68 km × 68 km broken cumulus cloud scene (Fig. 4a) from a less polluted region in Brazil, centered at 17°S and 42°W. The data were acquired on 9 August 2001 at 1015 LT. The solar zenith angle $\theta_0 = 41°$. This scene is part of phase 3 of the International Intercomparison of 3D Radiative Transfer Codes (I3RC; Cahalan et al. 2005) and has been used for the analysis of the retrieved droplet size by Marshak et al. (2006) and for the radiative effects of broken clouds on aerosol retrievals by Wen et al. (2007). The cloud fraction in the scene is $A_c = 0.4$. The MODIS image is collocated with a high–spatial resolution (15 m) Advanced Spaceborne Thermal Emission and Reflection Radiometer (ASTER) image (Yamaguchi et al. 1998) plotted in Fig. 4b. The
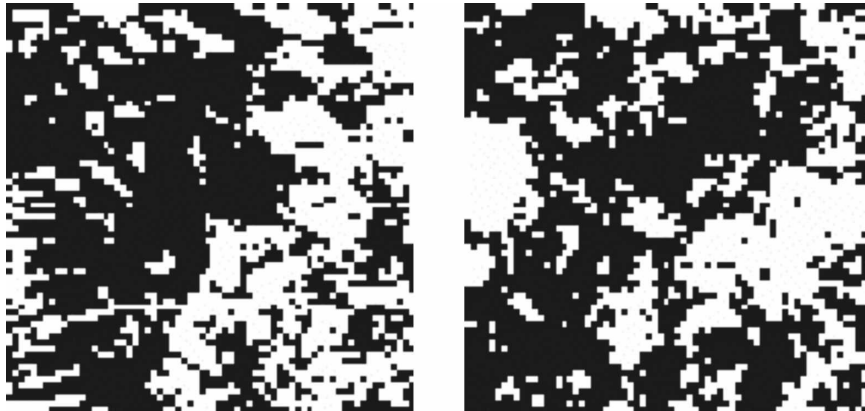
FIG. 5. Indicator functions $I(x, y)$ of a cloud field: white is cloud ($I = 1$) and black is a cloud-free area ($I = 0$). Cloud fraction $A_c = 0.4$. (left) A 68 km $\times$ 68 km MODIS image centered at (17.1°S, 42.16°W) acquired on 9 Aug 2001. (right) A realization of a simulated field.

solar azimuth angle $\varphi_0 = 23°$ (from upper right corner), as can be confirmed from the casting of the shadows.

In Figs. 4c and 4d we have also added the retrieved cloud optical depth and cloud-top height at a 1 km $\times$ 1 km resolution. Unlike the retrieved 1 km $\times$ 1 km cloud optical depth from the operational MODIS product, the operational cloud-top height retrievals have a 5 km $\times$ 5 km resolution (Platnick et al. 2003). To estimate the 1 km $\times$ 1 km resolution of cloud-top height, we used the brightness temperature at 11 μm (MODIS band 31) (see Wen et al. 2007 for details). As a result, Figs. 4c and 4d will serve as the basic scenes for our illustration.

First, Fig. 5a shows the indicator function $I(x, y)$ of the cloud optical depth field from panel 4c. The cloud fraction, as a mathematical expectation of I defined in (7), is 0.4. Figure 5b is the indicator function of a realization of a simulated field that has the same covariance function $K_I(x, y)$ as the measured one. As shown in appendix A, to get $K(x, y)$ we first estimated the covariance function K_I defined in (8) and then retrieved $K(x, y)$ with the help of the Owen function (Prigarin et al. 2004).

Next we illustrate how the distribution of cloud optical depth can be reproduced using Eq. (12a). This is done for model A, which perhaps agrees better with the observations than model B (Prigarin and Marshak 2005). Four realizations of cloud optical depth distribution are plotted in Fig. 6. All of them have approximately the same covariance function $K_I(x, y)$ of the indicator field (see Fig. 7) and probability density function (pdf) $g(\tau)$ as the original cloud optical depth field shown in Fig. 5c. Figure 8 illustrates these five pdfs: the original one and the four realizations of cloud optical depth from Fig. 6.

Now we illustrate the joint distribution of optical depth and cloud-top height. Figure 9 shows a joint distribution function; Fig. 10 shows an example of two conditional distributions $F(h|\tau)$ for $\tau = 3.5 \pm 0.5$ and $\tau = 10 \pm 1$. The conditional distributions of cloud-top height h are obviously different. Finally, Fig. 11 (for the realization of the cloud optical depth plotted in Fig. 6b) shows three realizations of cloud-top height. As we can see from Fig. 12, their pdfs match (approximately) the original pdf of cloud-top height from Fig. 4d.

7. Main steps of the model

Based on the above description, the software titled "Simulation of a two-component cloud field," which generates realizations of cloud optical depth and cloud-top height from given observations, has been developed and is freely available for download from http://i3rc.gsfc.nasa.gov/Public_codes_clouds.htm (click on "PDF-based stochastic cloud model").

Let us summarize here the main steps of the simulation procedure. There are only two input files: the cloud optical depth $\tau(x, y)$ and cloud geometrical thickness $h(x, y)$ (as shown in Figs. 4c and 4d). The main 11 steps are the following:

1. Read input file $\tau(x, y)$;
2. Estimate cloud fraction A_c [see (7)];
3. Find the truncation level d from (2);
4. Estimate the covariance function of the indicator field K_I [see (8)];
5. Compute the correlation function K (see appendix A);
6. Generate a Gaussian homogeneous random field $v(x, y)$ with mean zero and correlation function K (see appendix B);
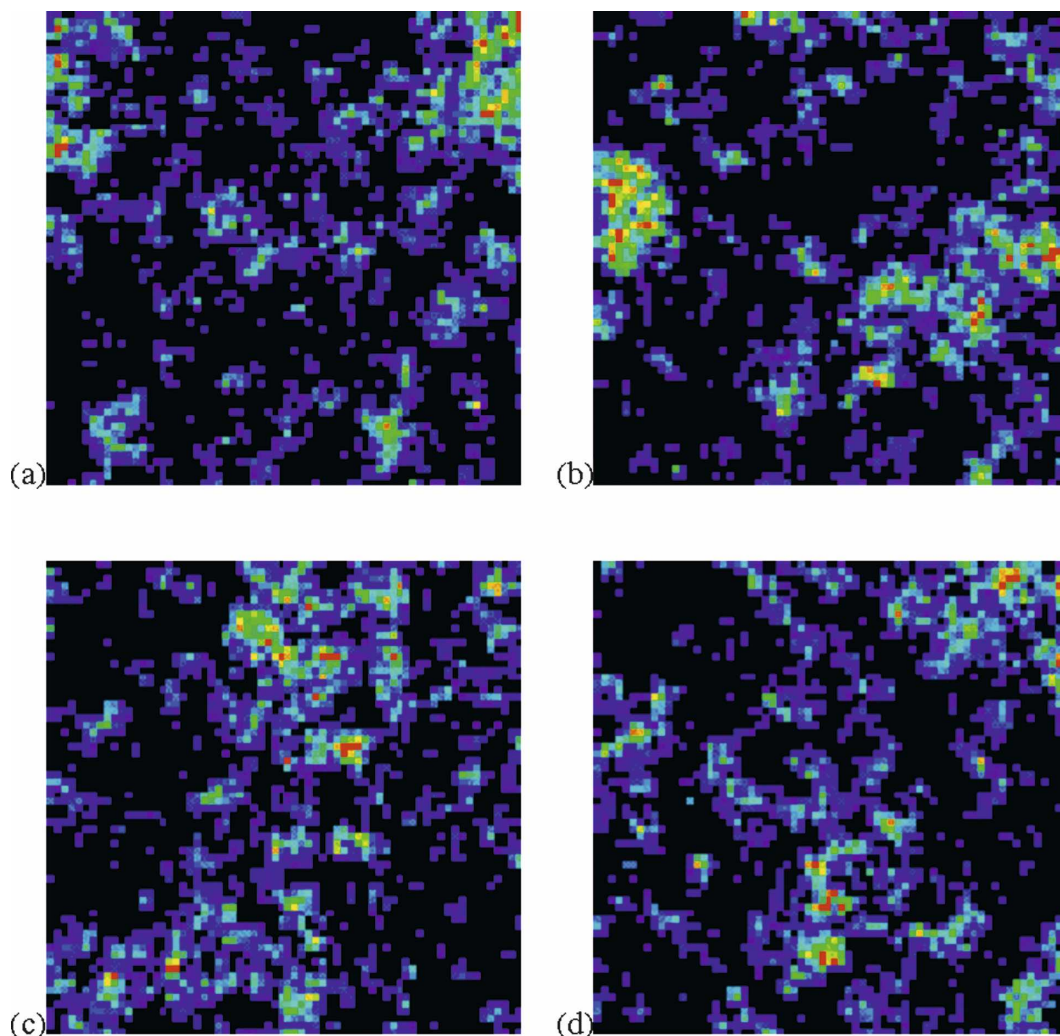
FIG. 6. Four realizations of cloud optical depth; all of them have the same covariance function of the cloud mask $K_I(x, y)$ and histogram $g(\tau)$ as the one in Fig. 4c. Color scale is as in Fig. 4c. The size of the images is 68 km × 68 km, as in Fig. 5.

7. Simulate $\tau^*(x, y)$, modifying the Gaussian field according to (12);
8. Read input file $h(x, y)$;
9. Calculate joint distribution of τ and h fields (see Fig. 9);
10. Calculate a conditional distribution matrix (13);
11. Using the conditional distribution matrix, simulate the realization $h^*(x, y)$ that corresponds to realization $\tau^*(x, y)$ generated at step 7 (see Fig. 11).

In the software, the first seven steps are accomplished by the executable file 0x-sp-a-s.exe. The input file is matrix $\tau(x, y)$. The output files are a realization $\tau^*(x, y)$ of cloud optical depth field, the estimated covariance function of the indicator field, the computed

autocorrelation function of the Gaussian field, and histograms of the input and output optical depth fields. The executable file DISTR-M2.exe estimates a joint distribution function of two random fields, $\tau(x, y)$ and $h(x, y)$. The output files of this program are the joint and conditional distributions (steps 8–10). For the last step, the executable file X_Ysim.exe is used. It provides a realization $h^*(x, y)$ of the cloud-top height field. In that way, the realizations $\tau^*(x, y)$ and $h^*(x, y)$ imitate the input fields $\tau(x, y)$ and $h(x, y)$ by reproducing the covariance function of the indicator field and joint distribution of τ and h components for the two-dimensional vectors $[\tau(x, y), h(x, y)]$. Note that here the random fields are assumed to be statistically homogeneous and isotropic.
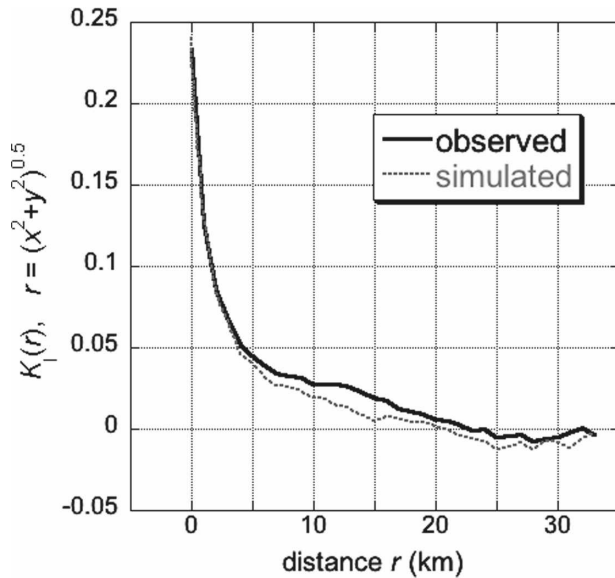
FIG. 7. Estimates of the covariance function $K_I(x, y) = K_I(r)$ ($r = \sqrt{x^2 + y^2}$) of the indicator function $I(x, y)$ for the observed (solid line) and simulated (dotted line) cloud fields from Fig. 5.

8. Summary

Cloud stochastic models have proved to be an important tool to study 3D radiative effects in clouds, especially in broken cumulus clouds (e.g., Barker and Davies 1992; Evans 1993; Marshak et al. 1998; Várnai 2000; Evans and Wiscombe 2004; Schmidt et al. 2007).
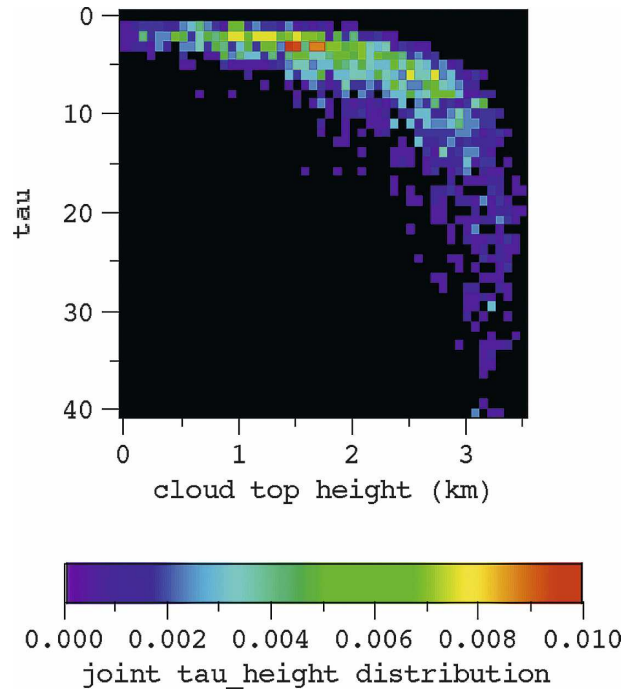

FIG. 9. Joint distribution of the given cloud optical depth and cloud-top height fields.

Here we have provided a theoretical description of a simple algorithm that generates realizations of the two correlated stochastic two-dimensional cloud fields that have statistical characteristics similar to given cloud fields. Each step of the algorithm has been illustrated
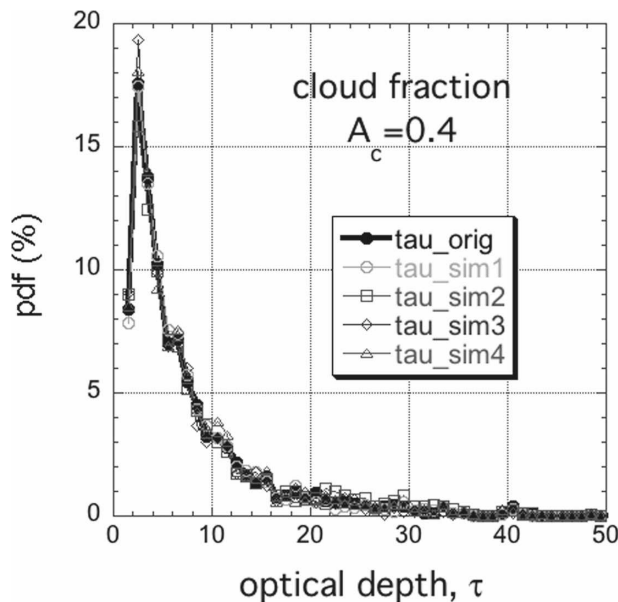

FIG. 8. The original histogram $g(\tau)$ and four other histograms that correspond to four realizations of cloud optical depth shown in Fig. 6.
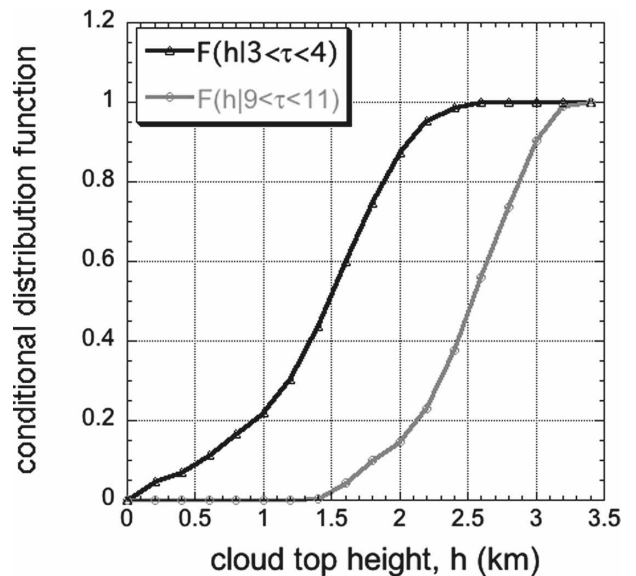

FIG. 10. The conditional distribution function $F(h|\tau)$ used to simulate cloud-top height h; $F(h|\tau)$ is shown for two values of optical depth τ.
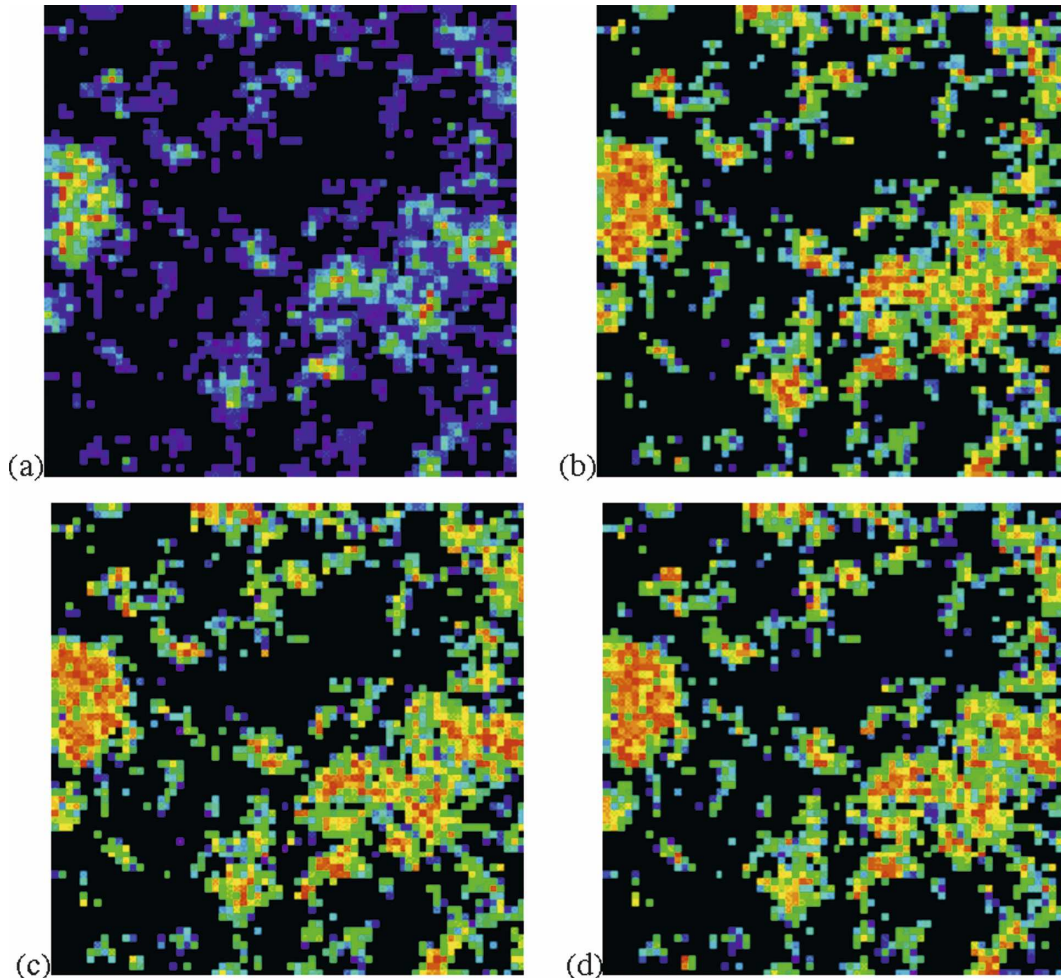
FIG. 11. (a) A realization of cloud optical depth from Fig. 6b. (b)–(d) Three additional realizations of cloud-top height distribution; they correspond to the cloud optical depth field shown in (a). All realizations have the same conditional distribution $F(h|\tau)$.

with two broken cumulus cloud fields: cloud optical depth and cloud-top height retrieved from MODIS. Whereas most stochastic cloud models use Fourier filtering of a Gaussian signal to generate the required correlation (e.g., Schertzer and Lovejoy 1987; Evans 1993; Di Giuseppe and Tompkins 2003; Evans and Wiscombe 2004; Hogan and Kew 2005; Venema et al. 2006b), our algorithm is based on spectral models of homogeneous random fields (Prigarin 1995, 2001). A nonlinear transformation of Gaussian functions (the method of inverse distribution function) allows us to keep the distribution function similar to the one of the first original field. Realizations of the correlated second field are generated using a conditional distribution matrix.

This paper is accompanied by the software "Simulation of a two-component cloud field," which has been recently released and can be freely downloaded from http://i3rc.gsfc.nasa.gov/Public_codes_clouds.htm. The software generates a two-component cloud field and provides programs to simulate two-dimensional distributions. The software contains a program (0x-sp-a-s) that generates realizations of a broken cloud field (X) with statistical characteristics (autocorrelation, density, and indicator functions) similar to the first given sample, a program (DISTR-M2) that estimates joint and conditional distributions for the two given samples, and a program (X_Ysim) that simulates a sample Y when a sample X is given. At present, the software runs only on Windows PCs but will be later extended to other platforms.

Finally we note that this model is a 2D stochastic model rather than 3D. To extend it to a 3D cloud model, we need to assume a vertical profile of cloud liquid water (see Di Giuseppe and Tompkins 2003). A simple linear increase of liquid water with height can be
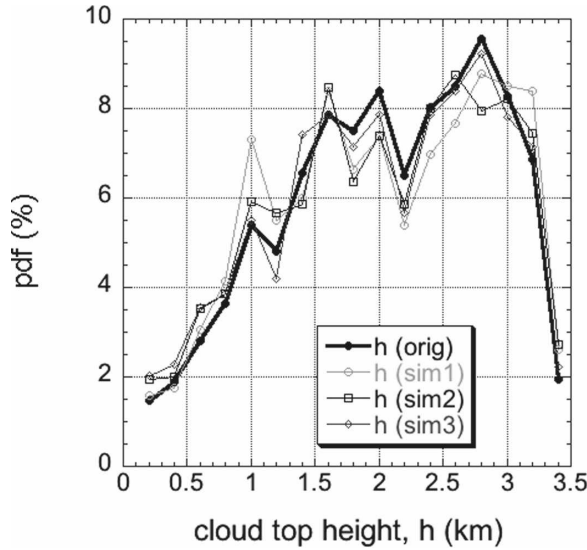
easily implemented in the frame of this model in its next stage.

APPENDIX A

Relations for Covariance Functions of a Gaussian Random Field and Its Indicators

Assume that $v(x, y)$ is a homogeneous Gaussian random field on the plane with mean zero and correlation function $K(x, y) = E[v(x, y) v(0, 0)]$. Let us consider two indicator fields with respect to a fixed level d:

$$I^{(1)}(x, y) = \begin{cases} 0 & \text{for} \quad v(x, y) < d \\ 1 & \text{otherwise,} \end{cases}$$

$$I^{(2)}(x, y) = \begin{cases} 0 & \text{for} \quad |v(x, y)| < d \\ 1 & \text{otherwise.} \end{cases}$$

These indicators correspond to model A (1a) and model B (1b) introduced in section 2. In this appendix we present the basic relations between covariance functions of the random field $v(x, y)$ and its indicators (for details, see Prigarin et al. 2004). For the covariance functions $K_I^{(n)}(x, y) = E[I^{(n)}(x, y) I^{(n)}(0, 0)] = P[I^{(n)}(x, y) = 1, I^{(n)}(0, 0) = 1]$ we have

$$K_I^{(n)}(x, y) = R^{(n)}[K(x, y)], \tag{A1}$$

where

$$R^{(1)}(r) = \int_{(\xi>d)} \int_{(\eta>d)} \varphi_r(\xi, \eta) \, d\xi \, d\eta,$$
$$R^{(2)}(r) = \int_{(|\xi|>d)} \int_{(|\eta|>d)} \varphi_r(\xi, \eta) \, d\xi \, d\eta, \tag{A2}$$

and

$$\varphi_r(\xi, \eta) = \left\{ 2\pi\sqrt{1 - r^2} \exp\left[\frac{\xi^2 + \eta^2 + 2r\xi\eta}{2(1 - r^2)} \right] \right\}^{-1} \tag{A3}$$

is the probability density of a two-dimensional Gaussian random vector with zero mean, unit variance of the components, and a correlation coefficient r between the components.

To find the correlation function $K(x, y)$ of the Gaussian random field for a quasi-Gaussian model of broken clouds, it is necessary to estimate function $K_I^{(n)}(x, y)$—i.e., the covariance function of the cloud indicator field—and to solve numerically Eq. (A1) ($n = 1$ for model A and $n = 2$ for model B). For computations it is reasonable to use the following representations of (A2) in terms of Owen's function:

$$R^{(1)}(r) = \Phi(-d) - 2T(d, a),$$
$$R^{(2)}(r) = 4\Phi(-d) - 4[T(d, a) + T(d, 1/a)], \tag{A4}$$

where Φ is the standard normal cumulative distribution function, $a = \sqrt{(1 - r)/(1 + r)}$, and

$$T(d, a) = \frac{1}{2\pi} \int_0^a \exp[-d^2(1 + u^2)/2] \frac{du}{1 + u^2} \tag{A5}$$

is Owen's function.

APPENDIX B

On the Simulation of a Gaussian Homogeneous Isotropic Field with a Given Correlation Function

Here we briefly present a numerical method used in the software "Simulation of a two-component cloud field" for modeling Gaussian random fields on a plane [for details, see chapter 2 in Ogorodnikov and Prigarin (1996); chapter 1, and particularly section 1.1.4, in Prigarin (2001); and Prigarin and Titov (1996)]. To simulate a Gaussian homogeneous isotropic random field $v(x, y)$ with mean zero and correlation function $K(x, y)$, we use an approximation of the following type:

$$v^{JM}(x, y) = M^{-1/2} \sum_{j=1}^{J} c_j \sum_{m=1}^{M} \sqrt{-2 \ln \alpha_{km}}$$
$$\times \cos(x\rho_j \cos\omega_{jm} + y\rho_j \sin\omega_{jm} + 2\pi\beta_{jm}),$$

where

$$\rho_j = (j + 0.5)B/J, \quad c_j^2 = \int_{(j-1)B/J}^{jB/J} z(\rho)\, d\rho,$$

$$\omega_{jm} = \pi(m + \gamma_j)/M, \quad \text{and} \quad z(\rho) = \rho \int_0^{\infty} r J_0(r\rho) K(r)\, dr,$$

$\alpha_{jm}, \beta_{jm},$ and γ_j are independent random variables uniformly distributed in $(0, 1)$, and the same symbol K is used for the correlation function (of the isotropic field) depending on a point on the plane (x, y) and on the distance $r = \sqrt{x^2 + y^2}$: $K(r) = K(x, y)$. Function $z(\rho)$ is the *radial spectral density* [see (6) in section 3]. Such numerical models are called *spectral models* because they approximate stochastic integrals in the spectral decomposition of the random field

$$v(x, y) = \int_0^{+\infty} \int_{-\infty}^{+\infty} \cos(\lambda x + vy)\xi(d\lambda\, dv)$$
$$+ \int_0^{+\infty} \int_{-\infty}^{+\infty} \sin(\lambda x + vy)\eta(d\lambda\, dv)$$

by finite sums. Here $\xi(d\lambda dv)$ and $\eta(d\lambda dv)$ are the orthogonal stochastic measures. [For the details on the spectral decompositions see, e.g., Gikhman and Skorokhod (1977, p. 273).] The spectral model is a sum of $J \times M$ random harmonics and it depends on three parameters J, M, and B, where B is an upper boundary of the radial spectrum of the model. (In the accompanying software "Simulation of a two-component cloud field," parameters J and M are chosen manually, whereas B is specified automatically). Additional information on the construction, properties, errors, and convergence of spectral models can be found in Prigarin (2001).

REFERENCES

Ackerman, A. S., O. B. Toon, and P. V. Hobbs, 1995: A model for particle microphysics, turbulent mixing, and radiative transfer in the stratocumulus-topped marine boundary layer and comparisons with measurements. *J. Atmos. Sci.,* **52,** 1204–1236.

Barker, H., and J. A. Davies, 1992: Solar radiative fluxes for stochastic, scale-invariant broken cloud fields. *J. Atmos. Sci.,* **49,** 1115–1126.

Cahalan, R. F., 1994: Bounded cascade clouds: Albedo and effective thickness. *Nonlinear Processes Geophys.,* **1,** 156–167.

——, and Coauthors, 2005: The I3RC: Bringing together the most advanced radiative transfer tools for cloudy atmospheres. *Bull. Amer. Meteor. Soc.,* **86,** 1275–1293

Di Giuseppe, F., and A. M. Tompkins, 2003: Effect of spatial organization on solar radiative transfer in three-dimensional idealized stratocumulus cloud fields. *J. Atmos. Sci.,* **60,** 1774–1794.

Evans, K. F., 1993: A general solution for stochastic radiative transfer. *Geophys. Res. Lett.,* **20,** 2075–2078.

——, and W. J. Wiscombe, 2004: An algorithm for generating stochastic cloud fields from radar profile statistics. *Atmos. Res.,* **72,** 263–289.

——, A. Marshak, and T. Várnai, 2008: The potential for improved cloud optical depth retrievals from the multiple directions of MISR. *J. Atmos. Sci.,* **65,** 3179–3196.

Gentle, J. E., 2003: *Random Number Generation and Monte Carlo Methods.* 2nd ed. Springer, 381 pp.

Gikhman, I. I., and A. V. Skorokhod, 1977: *An Introduction to the Theory of Random Processes* (in Russian). Nauka, 567 pp.

Hogan, R. J., and S. F. Kew, 2005: A 3D stochastic cloud model for investigating the radiative properties of inhomogeneous cirrus clouds. *Quart. J. Roy. Meteor. Soc.,* **131,** 2585–2608.

Kargin, B. A., and S. M. Prigarin, 1988: Modelling of stochastic fields of heap clouds and a study of their radiative properties with the Monte Carlo method (in Russian). Preprint 817, Siberian Division, USSR Academy of Sciences, Novosibirsk, 18 pp.

Marshak, A., A. Davis, R. F. Cahalan, and W. J. Wiscombe, 1994: Bounded cascade models as nonstationary multifractals. *Phys. Rev. E,* **49,** 55–69.

——, ——, W. J. Wiscombe, W. Ridgway, and R. F. Cahalan, 1998: Biases in shortwave column absorption in the presence of fractal clouds. *J. Climate,* **11,** 431–446.

——, S. Platnick, T. Várnai, G. Wen, and R. F. Cahalan, 2006: Impact of 3D radiative effects on satellite retrievals of cloud droplet sizes. *J. Geophys. Res.,* **111,** D09207, doi:10.1029/2005JD006686.

Ogorodnikov, V. A., and S. M. Prigarin, 1996: *Numerical Modelling of Random Processes and Fields: Algorithms and Applications.* VSP, 240 pp.

Platnick, S., M. D. King, S. A. Ackerman, W. P. Menzel, B. A. Baum, J. C. Riedi, and R. A. Frey, 2003: The MODIS cloud products: Algorithms and examples from *Terra. IEEE Trans. Geosci. Remote Sens.,* **41,** 459–473.

Prigarin, S. M., 1995: Spectral models of random fields and their applications. *Adv. Modell. Analysis,* **29A,** 39–51.

——, 2001: *Spectral Models of Random Fields in Monte Carlo Methods.* VSP, 198 pp.

——, and G. A. Titov, 1996: Spectral methods of numerical modeling of geophysical fields. *Atmos. Oceanic Opt.,* **9,** 629–635.

——, and A. Marshak, 2005: Numerical model of broken clouds adapted to observations. *Atmos. Oceanic Opt.,* **18,** 256–263.

——, and ——, 2008: Simulation of vector semibinary homogeneous random fields and modeling of broken clouds. *Numeric. Anal. Appl.,* **3,** 285–292.

——, B. A. Kargin, and U. G. Oppel, 1998: Random fields of broken clouds and their associated direct solar radiation, scattered transmission, and albedo. *Pure Appl. Opt.,* **7A,** 1389–1402.

——, A. Martin, and G. Winkler, 2004: Numerical models of binary random fields on the basis of thresholds of Gaussian functions. *Siberian J. Numer. Math.,* **7,** 165–175.

Scheirer, R., and S. Schmidt, 2005: CLABAUTAIR: A new algorithm for retrieving three-dimensional cloud structure from airborne microphysical measurements. *Atmos. Chem. Phys.,* **5,** 2333–2340.

Schertzer, D., and S. Lovejoy, 1987: Physical modeling and analysis of rain and clouds by anisotropic scaling multiplicative processes. *J. Geophys. Res.,* **92,** 9693–9714.

Schmidt, K. S., V. Venema, F. Di Giuseppe, R. Scheirer, M. Wendisch, and P. Pilewski, 2007: Reproducing cloud microphysics and irradiance measurements using three 3D cloud generators. *Quart. J. Roy. Meteor. Soc.,* **133,** 765–780.

Sveshnikov, A. A., 1968: *Applied Methods in Random Function Theory* (in Russian). Nauka, 463 pp.

Várnai, T., 2000: Influence of three-dimensional radiative effects on the spatial distribution of shortwave cloud reflection. *J. Atmos. Sci.,* **57,** 216–229.

Venema, V., S. Bachner, H. W. Rust, and C. Simmer, 2006a: Statistical characteristics of surrogate data based on geophysical measurements. *Nonlinear Processes Geophys.,* **13,** 449–466.

——, and Coauthors, 2006b: Surrogate cloud fields generated with the iterative amplitude adapted Fourier transform algorithm. *Tellus,* **58A,** 104–120.

Voss, R., 1985: Random fractal forgeries. *Fundamental Algorithms in Computer Graphics,* R. A. Earnshaw, Ed., Springer-Verlag, 805–835.

Wen, G., A. Marshak, R. F. Cahalan, L. A. Remer, and R. G. Kleidman, 2007: 3-D aerosol–cloud radiative interaction observed in collocated MODIS and ASTER images of cumulus cloud fields. *J. Geophys. Res.,* **112,** D13204, doi:10.1029/2006JD008267.

Yamaguchi, Y., A. B. Kahle, H. Tsu, T. Kawakami, and M. Pniel, 1998: Overview of Advanced Spaceborne Thermal Emission and Reflection Radiometer (ASTER). *IEEE Trans. Geosci. Remote Sens.,* **36,** 1062–1071.

Zuev, V. E., and G. A. Titov, 1995: Radiative transfer in cloud fields with random geometry. *J. Atmos. Sci.,* **52,** 176–190.